

# Hydrodynamics and Heat Transfer in Two and Three-dimensional Minichannels

D. Cherrared<sup>1</sup> and E. G. Filali <sup>1</sup>

**Abstract:** Our study deals with the characterization of the flow and related heat transfer in a smooth, circular minichannel. A duct with a sudden (sharp-edged) contraction is also considered. Prediction of the pressure loss coefficient in this case is obtained via the commercial code CFX 5.7.1. This code is based on the finite volume method for the solution of the Navier-Stokes and offers several turbulences models (in this study we use the shear stress turbulence model - SST). The numerical results are compared with experimental results obtained for a configuration similar to those considered in the numerical study. The numerical algorithm is also validated by comparison with [Reynaud, Debray, Franc, and Maitre (2005); Guo, Wang, Yu, Fang, Chongfang, and Zhuo (2010)]. A good agreement is obtained with the exception of the transition zone between laminar and turbulent regime. In the case of duct sudden contraction, the numerical results show that the abrupt contraction coefficient  $K_c$  decreases with the Reynolds number, and it is much higher than that of conventional tubes in laminar flow when the diameter  $D$  is less than 1mm.

**Keywords:** Hydrodynamics, friction factor, Heat transfer, loss coefficients, abrupt contraction, Minichannels

## 1 Introduction

During the last two decades, most of the studies on microchannels shows deviations with respect to traditional laws as unusual friction factors or shifts in the transition between laminar and turbulent flow. It is note worthy that several studies exhibit contradictory results for both mechanical and thermal characteristics of the flow. This is generally due to difference in the many parameters that characterize theses studies such as geometry (usually made of complex multichannels [Rahman (2000)]), the hydraulic diameter, the shape and surface roughness of the channels, the fluid nature, the boundary conditions, the flow regime but specially

---

<sup>1</sup> Faculty of Mechanical and Process Engineering, Houari Boumedienne University B.P. 32 El Alia, Algiers, Algeria

the measurements and calculating techniques itself. For a fundamental insight into microfluidics, it may then be useful to reduce as much as possible the number of parameters.

Judy, Maynes, and Web (2002) analyzed the laminar flow of water, methanol and isopropanol through circular and square sections. The results indicated that the friction factor  $f$  for square channels with diameters of  $47\mu m$  to  $101\mu m$  is in good agreement with conventional theory. In circular tubes with diameters varying from  $15\mu m$  to  $150\mu m$ , the friction factor  $f$  showed no significant deviation of the Poiseuille equation according to the experimental uncertainty.

Yang, Wu, Chien, and Lu (2003) studied the laminar and turbulent flows of water and a refrigerant liquid R-134a in smooth pipes with a diameter varying from  $0.502mm$  to  $4.01mm$ . The friction factor  $f$  for the two liquids is in conformity with the conventional equations; Poiseuille in laminar regime and Blasius in turbulent one.

Reynaud, Debray, Franc, and Maitre (2005) have realized experimental measurements of the friction factor and heat transfer coefficients in 2D minichannels of  $1.12mm$  to  $300\mu m$  in thickness. The minimum and maximum velocities recorded on all the tests are  $0.7$  and  $24 m/s$ . The friction factor is estimated from the measured pressure drop along the whole channel. The heat transfer coefficient is determined from a local and direct measurement of both temperature and heat flux at the wall using a specific transducer. They noted that the experimental results are in good agreement with classical correlations relative to channels of conventional size. The observed deviation were explained either macroscopic effects (mainly entry and viscous dissipation effects) or imperfections of the experimental apparatus. The application of micro-electro-mechanical systems (MEMS) have been increasing in many fields in recent years. Devices with dimensions of the order of microns are developed for micro-electronic cooling systems, bipolar plates of fuel cells and compact heat exchangers, etc. So far, a lot of researches have been conducted on micro-flow, most of which are focused on flow characteristics in straight channels due to frictional resistance.

Peng, Peterson, and Wang (1994) investigated the flow characteristics of water flowing through rectangular channel with a hydraulic diameter of  $133-367\mu m$ . It was found that the flow friction behavior for both the laminar and turbulent flow dramatically deviated from the classical correlations. The geometric parameters, hydraulic diameter, and the aspect ratio were found to be the most important parameters which had significant effects on the fluid flow through microchannels.

Liu and Grimella (2004) showed that conventional correlations offer reliable predictions for the Laminar flow characteristics in the rectangular microchannels over

a hydraulic diameter range of 244-974 $\mu\text{m}$ .

Qu and Mudawar (2002) performed experimental and numerical investigations of pressure drop and heat transfer characteristics of single phase laminar flow in 231 $\mu\text{m}$  and 713 $\mu\text{m}$  channels. Good agreement was found between the measurements and numerical predications, validating the use of conventional Navier-Stokes equation for microchannels.

Adams, Abdel-Khalik, Jeter, and Qureshi (1998) investigated the single-phase forced convection of water in circular microchannels of diameter 760 $\mu\text{m}$  and 1090 $\mu\text{m}$ . Their experimental Nusselt numbers were significantly higher than those predicted by traditional correlations. Adams, Abdel-Khalik, Jeter, and Qureshi (1999) extend this work to non-circular microchannels of large hydraulic diameters, greater than 1130 $\mu\text{m}$ . All their data for the large diameters were well predicted by the [Gnielinski (1976)] correlations, leading them to suggest a hydraulic diameter of approximately 1200 $\mu\text{m}$  as the lower limit for the applicability of standard turbulent single-phase Nusselt correlations.

The frictional resistance in straight channels, the local resistances in expansion, contraction, divergence, convergence and elbow also influences the total pressure drop in mini and microchannels. However, experimental studies on flow through a sudden flow area contraction in micro/mini channels are still lacking in the literature.

Abdelall, Hahn, and Ghiaasiaan (2005) performed several experiments to investigate pressure drops caused by abrupt flow area expansion and contraction in small circular channels. Fluids used are air and water at room temperature and near-atmospheric pressure. The diameters of larger and smaller tubes were 1.6 mm and 0.84 mm, respectively. The experimental results for water showed that approximately constant expansion loss coefficients occurred for turbulent flow in the smaller channel. The contraction loss coefficient for water was approximately 0.5 while that for air in turbulent flow was a constant and matched well with theoretical predictions. However, the expansion loss coefficients for air were not reported.

Chalfi and Ghiaasiaan (2008) measured pressure drops caused by flow area expansion and contraction under low flow conditions using air and water. The test sections consist of two capillaries with 0.84 mm and 1.6 mm diameters. The experimental expansion loss coefficients obtained for air is constant and equal 0.8 for  $Re \geq 5000$ . For  $Re < 600$ , the expansion coefficients for air and water had a sharp increase as the Reynolds number increased. The contraction loss coefficient for air in turbulent flow and water in laminar flow had a minor increase with the increase of Reynolds number.

Yu, Li, and C. F. Ma (2006) and Li, Yu, and Ma (2007, 2008) conducted experi-

ments with nitrogen and water, and investigated single-phase and gas-liquid two-phase pressure drops caused by a sudden contraction in microtubes at room temperature and atmospheric pressure. The diameter of the smaller tube is  $330\mu m$ . In single-phase flow experiments, the contraction loss coefficients for water are larger than the experimental results from conventional tubes in the laminar flow.

Our study consists in characterizing the dynamic and thermal field of a flow in smooth, circular minichannels. Predictions of the pressure loss coefficient in sudden contraction in the minichannels are also studied using a commercial code CFX 5.7.1. This code use the finite volume method to solve the equations of Navier-Stokes and offer several turbulences models. In this study, the shear stress turbulence model (SST) is used. The study of thermal field is not considered in sudden contraction, we were interested to dynamic field to compare the result with experimental measurements available in the literature for channels with conventional size.

## 2 Flow configuration and boundary conditions

Two configurations are considered in this study. The first configuration of the flow is a circular, smooth minichannel with a length  $L = 20cm$  and a variable diameter  $D$ . The fluid flow is coming through the entry ( $z = 0$ ), with a velocity  $U_e$ . The Reynolds number  $Re = U_e \cdot D / \nu$ , is based on the incoming velocity  $U_e$  and the minichannel diameter  $D$ . The selected flow conditions are taken as follow:  $U_e = 0.1$  to  $40m/s$  and  $D = 0.1$  to  $1mm$ .

The second configuration of the flow is the minichannels with sudden contraction. The Reynolds number  $Re_d = U_s \cdot d / \nu$ , is based on the output velocity  $U_s$  and the smaller minichannel diameter  $d$ . In order to predict reliably pressure losses in contractions, it is essential to understand the characteristic of feature flow for the whole range of geometries and flow conditions. The geometry range is defined by the contraction area ratio  $\sigma : 0 \leq \sigma \leq 1$ . In this work, two geometries were analyzed  $\sigma = 0.274$  and  $0.284$ . The choice of these values is imposed by the available experimental. The Reynolds number  $Re_d$  was varied from 700 to 6000. The geometry of the second configuration is illustrated on Figure 1.

We consider two configurations of the contraction (table 1), corresponding to different size of the diameter  $D$  and  $d$ .

Table 1: Two Study configurations

configurations	$\sigma$	$D(mm)$	$d(mm)$
1	0,274	2,10	1,10
2	0,284	0,60	0,32

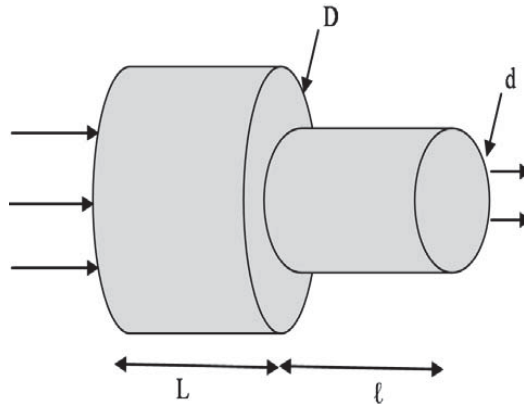


Figure 1: study domain ( $L = 5D$  and  $l = 40d$ )

$\sigma$  represent the flow area expansion function of the ratio ( $A_2/A_1$ ) and given as:  $\sigma = A_2/A_1 = (d/D)^2$ . With  $A_2$  and  $A_1$  represents the area corresponding to the diameter  $D$  and  $d$  respectively.

In all the study, the boundary conditions include a fully developed flow at inlet, mass conservation at outlet and no-slip at the wall surface. Automatic near-wall treatment is used for turbulence model SST. Automatic near wall treatment with automatically from wall functions to a low-Re near wall formulations as the mesh is refined. One of the well known deficiencies of the  $k - \varepsilon$  model is its inability to handle low turbulent Reynolds number computations. Complex dumping functions can be added to the  $k - \varepsilon$  model, as well as the requirement of highly refined near wall grid resolution ( $y^+ < 0.2$ ) in an attempt to model low turbulent Reynolds numbers flows. This approach often leads to numerical instability. Some of these difficulties may be avoided by using the  $k - \omega$  model, making it more appropriate than the  $k - \varepsilon$  model for flows requiring high near wall resolution. However, a strict low Reynolds number implementation of the model would also require a near wall resolution of at least  $y^+ < 2$ . This condition cannot be guaranteed in most applications at all walls. For this reason, a new near wall treatment was developed by CFX for the  $k - \omega$  based models that allows for a smooth shift from a low Reynolds number form to a wall function formulation. This near wall boundary condition, named automatic near wall treatment in CFX5, is used as the default in all models based on the equation (standard  $k - \omega$ , SST, etc).

In this study, the fluid is incompressible and Newtonian. The regime is stationary. The fluid used is water, incoming in the channel at temperature of  $20^\circ\text{C}$  and turbulence intensity of 5%. The following properties are used:  $\rho = 988.2\text{kg/m}^3$  and

$\nu = 1004.10^{-6}m^2/s$ . To simplify the study and to reduce number elements of the mesh volumes and to speed up the computation time, we opted for an axisymmetric geometry for the first configuration.

Our calculations are compared to classical results in the laminar and turbulent regimes. For the laminar regime, it can be shown analytically that, in the case of a fully developed flow, the Poiseuille number is constant ( $P_0 = 24$ ).

### 3 Numerical technique

The fundamental equations governing the flow phenomenon are the general equation of mass, momentum and energy. The resolution of these differential equations requires the choice of a suitable numerical method to solve the problem. For our case, we choose the finite-volume method. The turbulence model used is the SST model (Shear stress turbulence model) [Menter (1994)

We specially pay attention in selected grid. The mesh employed is of tetrahedral elements with prismatic refining at the wall, illustrated in figures 2 and 3.

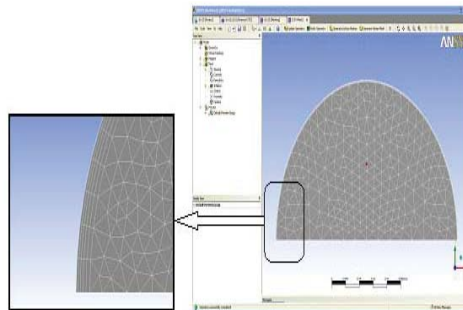


Figure 2: Transverse section (first configuration)

Non uniform grid was generated and grid refinement close to the wall and sudden contraction zone was applied. Several successive grid refinements have been carried out in every case to get negligible effect of the mesh in the solutions. The mesh obtained is of 1.2 million nodes and 6 million tetrahedral elements.

The CFD used is a combination of two complementary software: The Workbench 9.0 processor, which makes it possible to prepare the geometry and to generate grid and the CFX solver, who solves the equations modeling the phenomenon.

The CFX solver finishes the calculations when the equation residuals calculated using the specified method is below the target residual value. A convergence criterion of  $10^{-3}$  is used to ensure negligibly small iteration errors (figure 4).

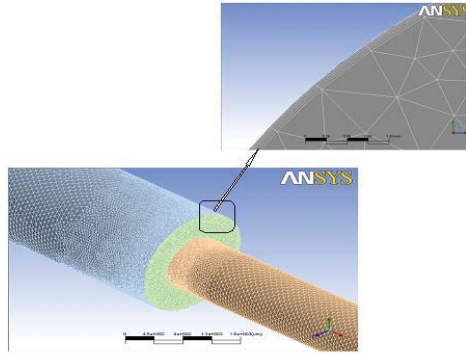


Figure 3: Computational geometry (second configuration)

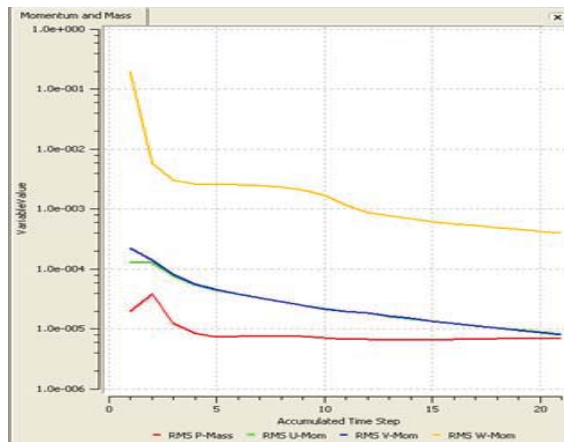


Figure 4: convergence curves

## 4 Results and discussion

### 4.1 Flow in a smooth circular minichannels

Our simulations are of a hydrodynamic aspects and heat transfer. We looked, in particular; the velocity profiles, boundary layer thickness, the lengths of fully developed flow, the frictions factors as well as the pressure drop. Those parameters are analyzed in respect of; the effect of Reynolds number variation as well as the variation of the diameter of the minichannels. The variation of the Nusselt number is also studied. The obtained results are compared to the classical correlation applied for the pipe with conventional size. A comparison with experimental results is also conducted.

#### 4.1.1 Effect of the variation of the Reynolds number

In this part, we present the results obtained in a minichannel of diameter  $D = 1mm$ , while the length of the pipe  $L$  is  $20cm$ . The velocity of the incoming flow varies from  $0.1$  to  $40m/s$ .

Figures 5 and 6, shows the evolution of the velocity profiles in a section located at  $z = 10cm$  from the entry of the minichannel. Values of the Reynolds number, going from  $5000$  to  $40000$ , in the case of a turbulent flow and between  $100$  to  $1000$  for the laminar regime. It should be noted that we take care so that all the data are recorded in a fully developed flow.

For the two regimes, we observe an increase of the maximum velocity at the center of the minichannel, with the increase of the Reynolds number. This increase is linear as shown in figure 7.

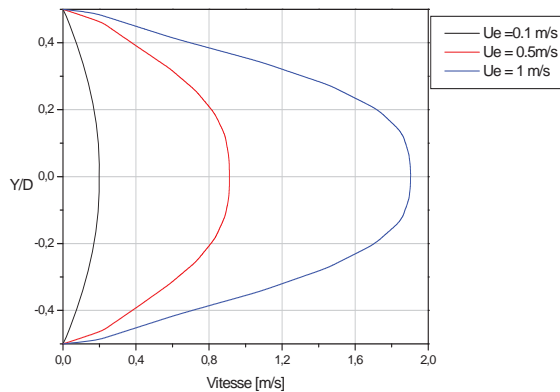


Figure 5: Velocity profiles, laminar flow

The ratio  $U_{max}/U_e$  is equal to  $1.30$  for velocities between  $5$  and  $40m/s$  (turbulent flow), and  $1.92$  for velocities of  $0.1$  to  $1m/s$  (laminar flow). For the classical pipes, the theory gives for the same ratio; the value  $1.2$  for the turbulent flow, and  $2$  for laminar one.

The results obtained, seems to be in general agreement with those previously reported by the theory of the classic pipes.

The literature provides that in the case of the channel with classic size, the hydrodynamic length of fully developed flow is function of the diameter of the pipe and the Reynolds number for a laminar regime, and only function of the diameter of the pipe when the flow is turbulent, as mentioned:

Laminar flow:  $L_e/D \approx 0.01.Re$

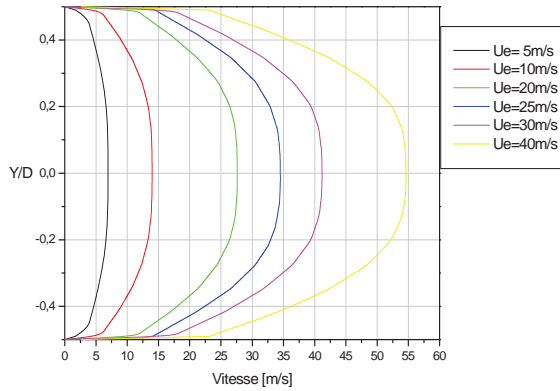


Figure 6: Velocity profiles, turbulent flow

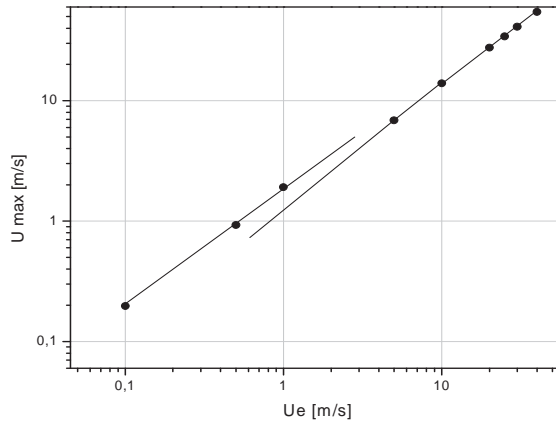


Figure 7: Evolution of maximum velocity at the center of minichannel

Turbulent flow:  $Le/D \approx 25 - 40$  [Schlichting and Gersten (2004)]

From our calculations, the variation in the length of fully developed flow according to the Reynolds number is represented figure 8, for  $D = 1mm$ . The same characters are observed in the case of minichannels compared to the classic theory. Indeed, we observe that the length of fully developed flow increases in a linear way according to the Reynolds number for the low values. After a zone of transition located between 1000 and 5000, we observe a stabilization of the curve, meaning the independence of this length according to the Reynolds number. The calculation of the ratio  $Le/D$  gives a value of  $0.018 Re$  for laminar flow. This result is in good agreement with the theory of pipe with conventional size equation above. For a turbulent

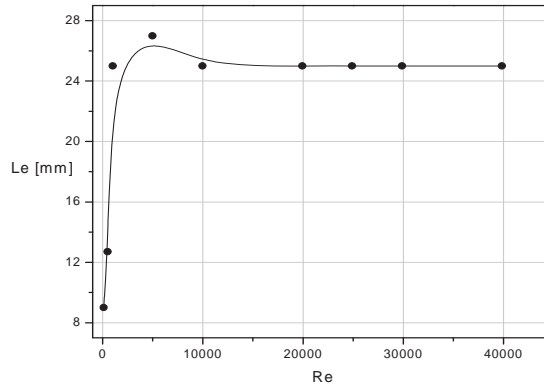


Figure 8: Length of fully developed flow

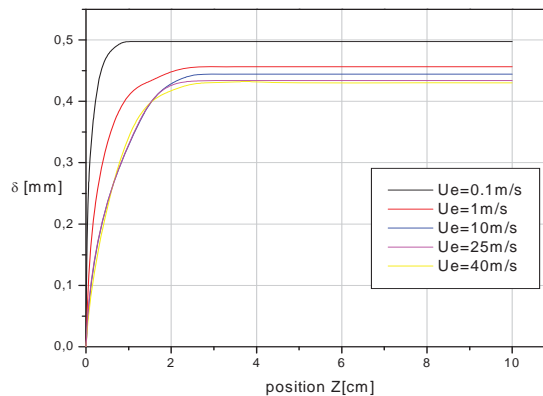


Figure 9: Evolution of the dynamic boundary layer

flow, this ratio is equal to 25, value proposed by the classical theory [Schlichting and Gersten (2004)].

The transition zone seems to be located between (1000 and 5000); which means, that this zone is different from that predicted for the classic pipes. This observation is also underlined by some authors [Reynaud, Debray, Franc, and Maitre (2005)].

Figure 9, represent the evolution of the hydrodynamic boundary layer through the minichannel. We can note the existence of a zone of strong velocity gradient causing the formation of the boundary layer whose value seems to be stabilized when the flow is fully developed. The order of magnitude of this boundary layer thickness, varies between 0.499 and 0.43 respectively for velocity equal to 0.1 (laminar

flow) and  $40\text{m/s}$  (turbulent flow); as maximum value. For laminar flow, the boundary layer invade practically all the minichannel, for turbulent one, the boundary layer covers only one percentage of the diameter of the minichannel.

In the case of the turbulent regime, the zone of flatness decreases when the Reynolds number increases, showing the inverse relation between the thickness of boundary layer  $\delta$  and the Reynolds number ( $\frac{\delta(z)}{z} = \frac{C_1}{Re_x^{1/5}}$  where;  $C_1 \in [0.2, -0.3]$ ); the traditional laws give a value of 0.37 for the constant  $C_1$ .

The friction factor is estimated from the calculated pressure drop. The pressure drop is calculated between two sections of the inlet and outlet of the minichannel. Figure 9 schematizes the variation of the friction factor according to the variation of the Reynolds number. While referring to the theoretical results of the classic pipes, the laws are:

Laminar flow:

$$\lambda = \frac{64}{Re} = 4C_F \quad (1)$$

Turbulent flow:

$$C_F = \frac{\lambda}{4} = \frac{0.079}{Re^{1/4}} \quad (2)$$

From the equilibrium of forces on a portion of fluid of length  $L$  and diameter  $D$  subjected to a pressure difference  $\Delta P$  (assuming a hydrostatic pressure distribution), we write the relation (3) that links the parietal shear stress. We obtain the relation (4) which allows us to calculate the friction coefficient.

$$\tau_p = \frac{1}{2}\rho U_m^2 C_f = \frac{\Delta P \cdot D}{4L} \quad (3)$$

$$C_F = \frac{\Delta P \cdot D}{2L\rho U_m^2} \quad (4)$$

Results are reported in figure 10, which shows a good agreement between the results of simulations and the formulas drawn from the classic theory.

We observe a reduction in the friction factor according to the inverse of the Reynolds number for the laminar flow, and an evolution in  $1/Re^{1/4}$  for the turbulent flow. This result is confirmed by figure 11, the increase in the Reynolds number is accompanied by an increase in pressure drop according to two different rapports: laminar; 67 and turbulent; 150. The order of magnitude of the pressure drop is in the allowed beach of the values. The experiment recommends value between 15 and 20 bars for velocity of  $30\text{m/s}$  in the minichannel.

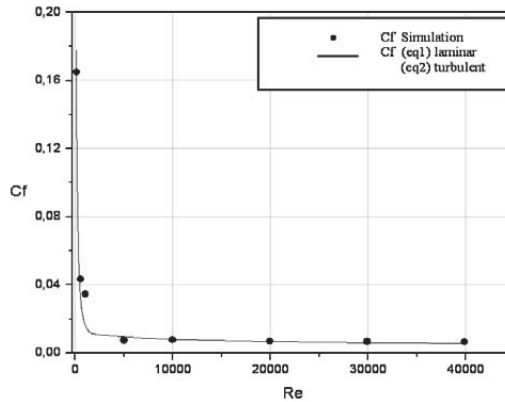


Figure 10: Friction factor vs Reynolds number

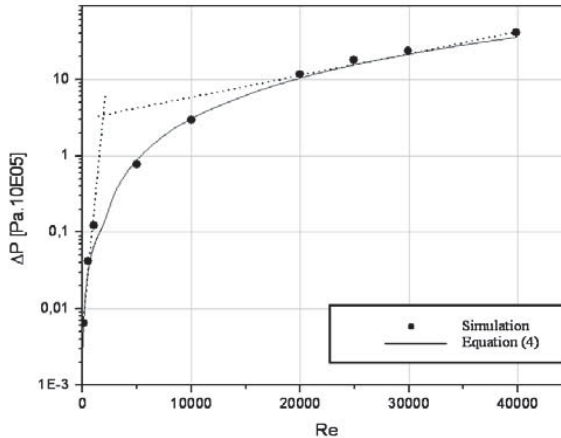


Figure 11: Pressure drop vs Reynolds number

#### 4.1.2 Effect of variation of the minichannel diameter

We report figure 12, the evolution of the length of fully developed flow according to the diameter of the minichannel. The calculation for incoming velocity  $U_e = 10m/s$  are compared to those for  $U_e = 25m/s$ . We can note that the length of fully developed flow is not influenced by the change of the Reynolds number, result also predicted by the classical theory. The calculation of the slope of the linear curve gives the value of 25, value observed previously by the calculations and also obtained by experimental results.

The curve of figure 13 gives the evolution of the average friction factor according

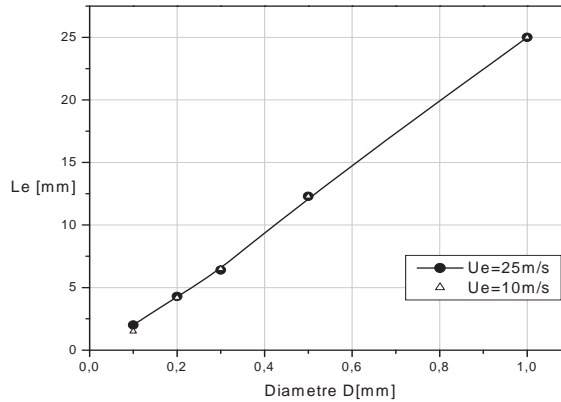


Figure 12: Evolution of the length of fully developed flow

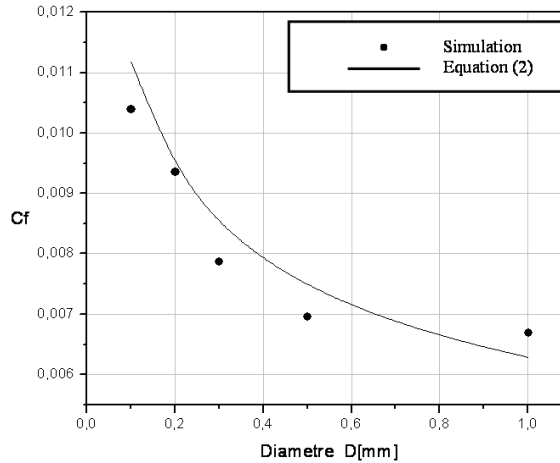


Figure 13: Evolution of the friction factor vs the diameter

to the diameter of the minichannel, for incoming velocity,  $U_e = 25m/s$ . The curve shows some divergences between the numerical results and traditional laws for the pipes of classic sizes. It seems that this difference is due to the calculation of the total friction factor. Indeed, this coefficient is only an average of the values of the local friction factor over a given length. It is to note, that the length of the minichannels is not constant in all cases, to reduce computational time.

Table 2 shows the variation of the minichannel length various diameter. These values are obtained after many tests to have an optimal length of the minichannel for calculation, but we have to be some that results are released in fully developed

flow.

Table 2: variation of the minichannel length vs diameter

$D$ (mm)	1	0.5	0.3	0.2	0.1
$L$ (cm)	20	10	5	5	2

#### 4.1.3 Comparison with experimental results

A comparison between our numerical results, experimental ones and traditional laws, is made. The comparison is about the evolution of the Poiseuille number with the Reynolds number, figure 14, for Diameter  $D = 1\text{mm}$ .

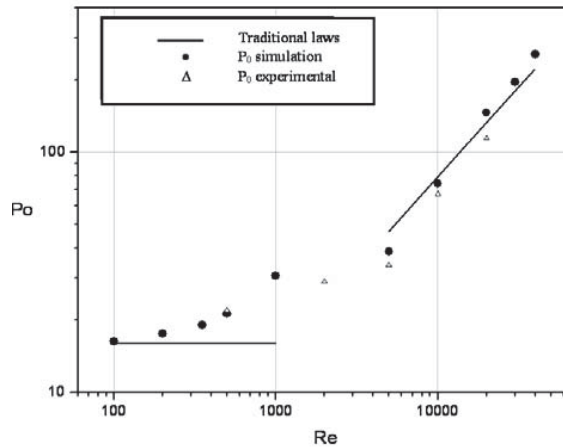


Figure 14: Poiseuille number vs Reynolds number

We can observe for Reynolds number  $Re < 1000$  (laminar flow), that the Poiseuille number evolve with Reynolds number and is higher than that previous by the classic laws. Indeed, for the laminar regime, it can be shown analytically that, in the case of fully developed flow, the Poiseuille number is constant  $P_o = 24$ . These results seem on the other hand close to the experimental values (Reynaud). It would seem that the increase of the dynamic length of fully developed flow with the Reynolds is at the origin of this phenomenon.

For  $Re > 5000$ , the Poiseuille number is of the same order of magnitude as the value given by traditional laws. For the fully developed turbulent regime, and in the case

of smooth wall, the Poiseuille number can be approximated by the traditional empirical relation:  $P_o = 0.079R_e^{0.75}$ . The results obtained, are close to the experimental ones.

We observe that the evolution of the Poiseuille number undergoes a break of slope for a Reynolds number ranging between 1000 and 5000. This change can be interpreted as the transition from the laminar regime to the turbulent one.

#### 4.1.4 Heat transfer results

In this part, we present the effect of the variation of the Reynolds number on the heat transfer in a minichannel of diameter  $D = 0.3mm$ . The length of the minichannel is  $L = 5cm$ . The heat flux applied to the wall of the minichannel is  $100000w/m^2$ .

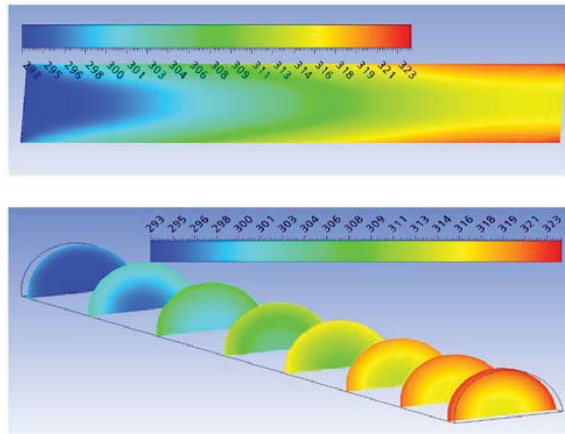


Figure 15: Evolution of the temperatures

Figure 15, shows the evolution of temperature along the wall of the minichannel. We note an increase of the temperature along the mini-channel. The development of the thermal boundary layer, which, as well as for the dynamic one, follows a higher evolution.

We represent, figure 16, the evolution of the thickness of dynamic and thermal boundary layer along the mini channel. The analysis of the results gives a mean value of the report  $\delta_{th}/\delta$  equal to 0.96. To note that this value is twice as big as that given by the classic theory ( $\delta_{th}/\delta = 1/\text{Pr}^{1/2} = 0.4$ ). It seems, that classical theory are not recommended for minichannel when the diameter is less than 1 mm. Observations already made by others authors [Reynaud, Debray, Franc, and Maitre (2005)].

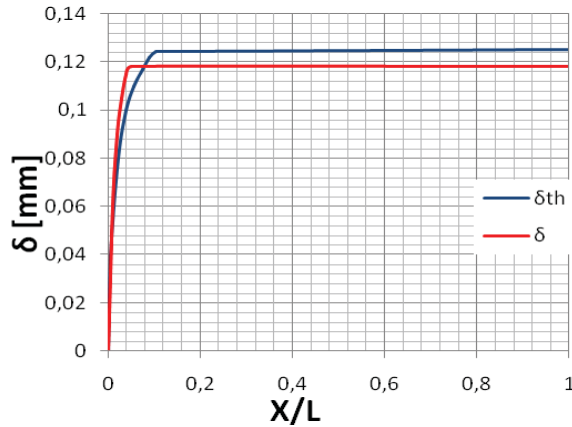


Figure 16: Evolution of the thermal boundary layer

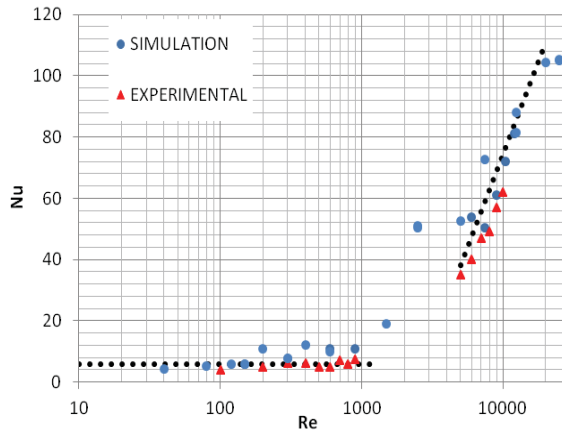


Figure 17: Nusselt number vs Reynolds number

Figure 17 represents the variation of the average Nusselt number according to the Reynolds number. The increase of the Reynolds number causes the increase of the average Nusselt number. This means the intensification of inertial force to overcome the effect of the viscous ones. This increase of inertial force accelerates the movement of particles near the wall so allowing an increase of the heat transfer by convection and so, a decrease of the temperature at this level.

The validation of our calculations is made by a comparison with the theoretical values established for the classic channels, and experimental measurements were obtained for a minichannel with similar dimensions to those of our study. A good

concordance is observed, with regard to the works realized in minichannels, we shall note however, that some deviations are visible with regard to the results obtained with classic correlations. In particular, concerning the evolution of the Nusselt number. Indeed, the values issues from simulations, shows a light evolution of the Nusselt number in laminaire flow, what is not the case for the classic correlations which predict a constant Nusselt number equal to 5.38. Concerning the turbulent flow, the orders of the Nusselt number are preserved, compared with those obtained by the classic theory ( $Nu = 0.023R_e^{0.8} Pr^{1/3}$ : Colburn equation); While our calculations gives 0.026 for the numerical constant.

We shall note however, that a some deviations are observed for the transition laminar-turbulent zone. This zone seems to be situated for values of Reynolds number going from 1000 to 5000. These values shows that the passage between the laminar flow to the turbulent one is made in a more precise way than the classic theory denote it. This result is also observed by numerous researchers working in the field of the mini and microchannels.

#### 4.2 Flow through minichannel with sudden contraction

Flow through channels with sudden contraction occurs in many industrial applications. The flow separation in the vicinity of the contraction plane causes an increase in pressure loss, which affects erosion rates and heat and mass transfer at the separation and reattachment regions.

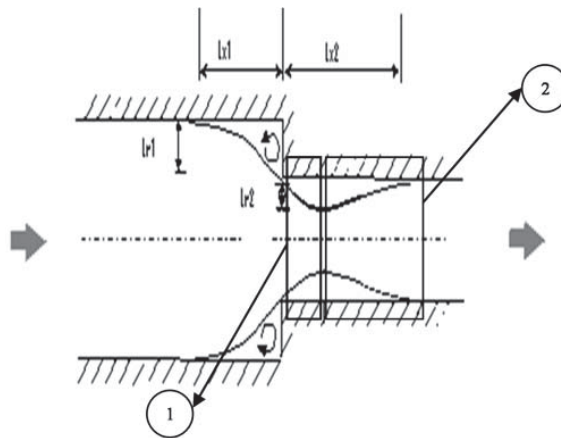
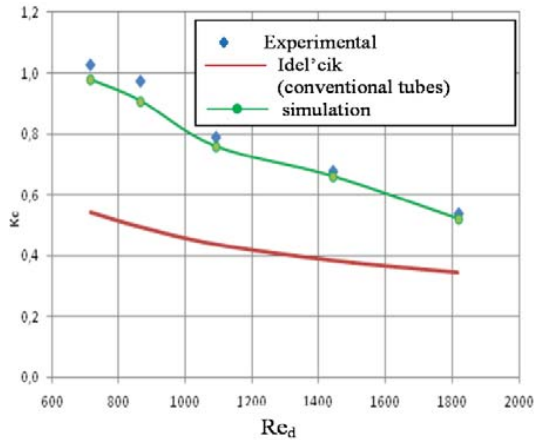
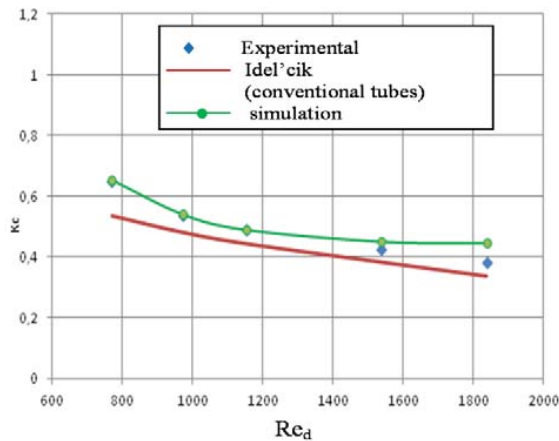


Figure 18: Schematic of the flow through a pipe with a sudden contraction

In this part the values of Reynolds numbers considered are between 700 and 6000.

a) ( $D=0.6\text{mm}$ ,  $d=0.32\text{mm}$ ,  $\sigma=0.284$ )b) ( $D=2,10\text{mm}$ ,  $d=1,10\text{mm}$ ,  $\sigma=0.274$ )Figure 19: Contraction loss coefficient  $K_c$  (Laminar flow)

The CFD predictions of the pressure loss coefficient for this geometry and flow configurations are compared with the measurements for laminar and turbulent flow of Guo, Wang, Yu, Fang, Chongfang, and Zhuo (2010).

The pressure loss through the contraction is caused by two consecutive processes: (1) contraction of the flow to the vena contracta, and (2) expansion to the wall of the small pipe (figure 18). The latter is an “uncontrolled” expansion against an adverse pressure gradient. In order to determine the overall pumping power in a piping system (minichannel), it is essential to have reliable design procedures to

predict pressure losses. It is also important to know the flow details of the separations upstream and downstream of the contraction plane to avoid placing sensitive equipment in these regions (figure 18)

The pressure loss coefficient for a sudden contraction is defined as

$$K_c = \frac{\Delta P_{t12}}{1/2\rho U_2^2} \quad (5)$$

Where  $\Delta P_{t12}$  is the total pressure drop due to the contraction, and  $1/2\rho U_2^2$  is the kinetic pressure at Station 2.  $\Delta P_{t12}$  is defined as the total pressure drop between Station 1 in the large pipe and Station 2 in the small pipe. Station 1 and 2 are located in the fully developed regions upstream and downstream of the contraction respectively, outside the region of influence of the contraction.

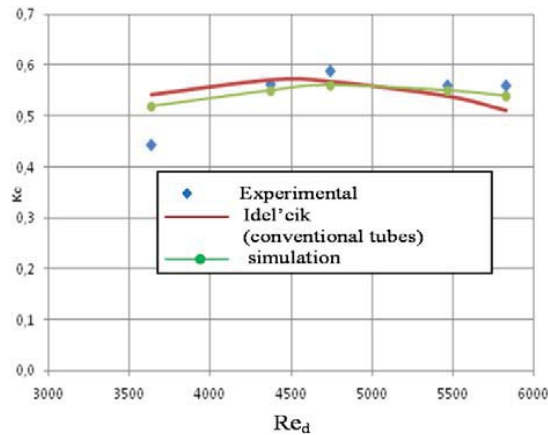
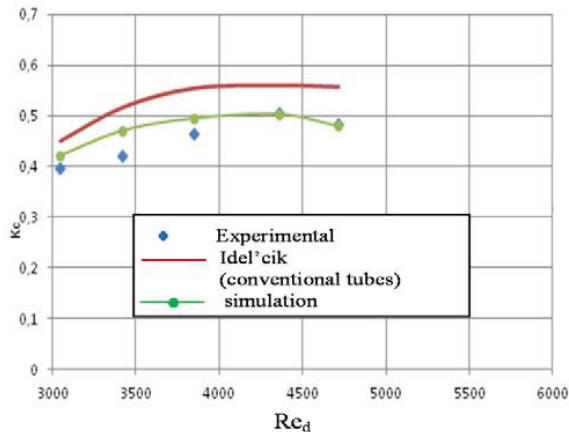
When a fluid flows through a sudden contraction, the mechanical energy loss takes place predominantly during the deceleration following the vena-contracta.

The variation of the sudden contraction loss coefficients in laminar region are shown in Figure 19. In the laminar flow region, the numerical results indicate that  $K_c$  decreases with  $Re_d$  increasing and it is much higher than that of conventional tubes [Idel'cik (1986)].

When the diameter increases,  $K_c$  decreases and the difference between the experiment results and Idel'cik's results becomes smaller. There is a good agreement between the experimental and numerical results (CFX) in mini-channels. According to the equation of contraction loss coefficient (eq. 5), we can explain the decrease of  $K_c$  by the important increase of velocity compared to that of the pressure difference  $\Delta P$ .

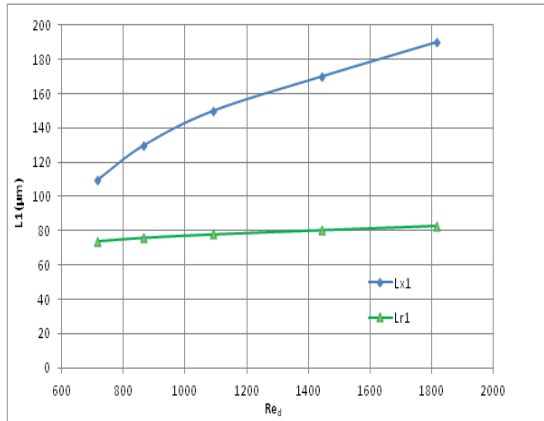
The sudden contraction loss coefficients for turbulent regime are shown in Figure 20. The numerical results indicate that  $K_c$  increases to a maximum value and then it decreases slightly with  $Re_d$  increasing. The curve of  $K_c$  shows a smaller gap with that of the conventional tube. When the diameter increases, the  $K_c$  from the numerical data does not change while  $Re_d$  increasing. There is enough good agreement between the experimental and numerical results (CFX) in minichannel.

The CFD predictions of the upstream and downstream separation regions for  $700 \leq Re_d \leq 6000$  are shown in figures 21 and 22. Predictions using CFX code display similar trends. These trends show an increase of the separation length and height. The variation of the separation length is greater than the height variation. However, in turbulent flow, the separation length downstream of contraction decreases while  $Re_d$  increasing. This can be due to the appearance of a small vortex at the corner of the contraction, which can also affect the size of the downstream separation length.

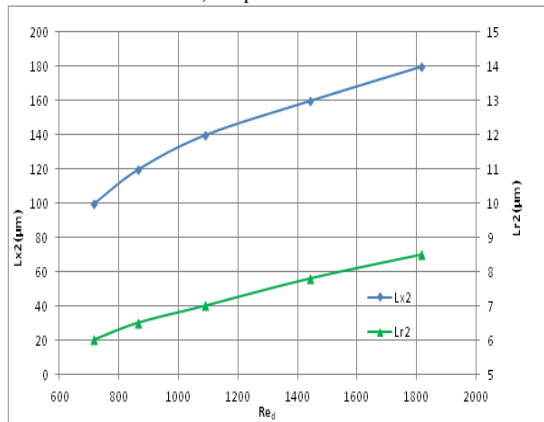
a) ( $D=0.6\text{mm}$ ,  $d=0.32\text{mm}$ ,  $\sigma=0.284$ )b) ( $D=2,10\text{mm}$ ,  $d=1,10\text{mm}$ ,  $\sigma=0.274$ )Figure 20: Contraction loss coefficient  $K_c$  (Turbulent flow)

## 5 Conclusion

Simulations are made with the commercial code CFX5.7.1 were conducted in minichannels. Dynamics aspect and heat transfer are analyzed on one size diameter of minichannel. Effect of the local resistance of flow across sudden contraction is also studied. In the results obtained are rich in information for the dynamic aspects and heat transfer the parameters are Reynolds number, diameter of the minichannel, Poiseuille number, boundary layer and Nusselt number. In addition to the results



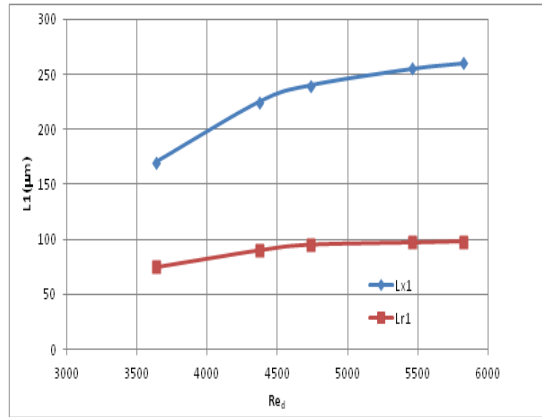
a) upstream



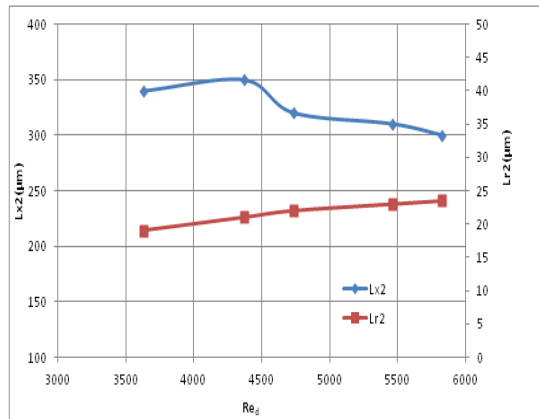
b) downstream

Figure 21: Separation length  $Lx$  and height  $Lr$  predicted by CFX at different  $Re_d$  (Laminar flow,  $D=0.6mm$ ,  $d=0.32mm$ ,  $\sigma=0.284$ )

from the theory, established for the traditional pipes, we have experimental results obtained for a minichannel of size similar to those of our study. The validation of our calculations is thus made by a comparison with experimental measurements [Reynaud, Debray, Franc, and Maitre (2005)] and theoretical values. A good agreement is observed, note however that a slight deviation is observed concerning the transition zone between laminar and turbulent regime. This zone seems to be located for values of Reynolds number going from 1000 and 5000. This result was confirmed by many researchers working in the field of the mini and microfluidics. These values show that the transition zone is more precisely pointed than the classical theory predicted it. The results of this study are not likely to give in cause



a) upstream



b) downstream

Figure 22: Separation length  $Lx$  and height  $Lr$  predicted by CFX at different  $Re_d$  (Turbulent flow,  $D=0.6mm$ ,  $d=0.32mm$ ,  $\sigma=0.284$ )

validity of the traditional laws in the case of the mini-channels until a diameter of  $0.1mm$ . We showed that deviations are observed compared to the traditional correlations, but generally, a good agreement is noted.

Concerning the sudden contraction, in the laminar flow region, the contraction coefficient  $K_c$  decreases with  $Re_d$  increasing. The  $K_c$  from the numerical result of minichannel decreases as the diameter increases. When the diameter increases, the difference in  $K_c$  between the numerical results on minichannel and the correlation with conventional tubes becomes smaller. The numerical study showed that the results of pressure loss coefficient are almost superposed with the experimental ones

[Guo, Wang, Yu, Fang, Chongfang, and Zhuo (2010)].

**Acknowledgement:** The authors would like to acknowledge the support provided by the United Arab Emirates University. This work was financially supported by the Research Affairs at the university under a contract no. 01-05-7-11/09.

## References

- Abdelall, F. F.; Hahn, G.; Ghiaasiaan, S. M.** (2005): Pressure drop caused by abrupt flow area changes in small channels. *Experimental Thermal and Fluid Science*, vol. 29, no. 4, pp. 425–434.
- Adams, T. M.; Abdel-Khalik, S. I.; Jeter, S. M.; Qureshi, Z. H.** (1998): An experimental investigation of single-phase forced convection in microchannels. *Int. J Heat Mass Transfer*, vol. 41, no. 6-7, pp. 851–857.
- Adams, T. M.; Abdel-Khalik, S. I.; Jeter, S. M.; Qureshi, Z. H.** (1999): Applicability of traditional turbulent single-phase forced convection correlations to non-circular microchannels. *Int. J Heat Mass Transfer*, vol. 42, no. 23, pp. 4411–4415.
- Chalfi, T. Y.; Ghiaasiaan, S. M.** (2008): Pressure drop caused by flow area changes in capillaries under low flow conditions. *International Journal of Multiphase Flow*, vol. 34, no. 1, pp. 2–12.
- Gnielinski, V.** (1976): New equations for heat and mass transfer in turbulent pipe and channel flow. *Int. Chem. Eng.*, vol. 16, no. 2, pp. 359–368.
- Guo, H.; Wang, L.; Yu, J.; Fang, Y. E.; Chongfang, M. A.; Zhuo, L. I.** (2010): Local resistance of fluid flow across sudden contraction in small channels. *Front. Energy Power Eng. China*, vol. 4, no. 2, pp. 149–154.
- Idel’cik, I. E.** (1986): *Handbook of Hydraulic Resistance*. Hemisphere Publishing Corporation, New York, 2nd edition.
- Judy, J.; Maynes, D.; Web, B. W.** (2002): Characterisation of frictional pressure drop for liquid flows through microchannels. *International Journal of Heat and Mass Transfer*, vol. 45, no. 17, pp. 3477–3489.
- Li, Z.; Yu, J.; Ma, C. F.** (2007): Local resistances of single-phase flow across abrupt expansion and contraction in small channels. *Journal of Chemical Industry and Engineering*, vol. 58, no. 5, pp. 1127–1131.
- Li, Z.; Yu, J.; Ma, C. F.** (2008): Characteristics of pressure drop for single-phase and two-phase flow across sudden contraction in micro tubes. *Science in China Series E*, vol. 51, no. 2, pp. 162–169.

**Liu, D.; Grimella, S. V.** (2004): Investigation of liquid flow in microchannels. *AIAA J. Thermophys. Heat Transfer*, vol. 18, pp. 65–72.

**Menter, F. R.** (1994): Two-equation eddy-viscosity turbulence models for engineering applications. *AIAA Journal*, vol. 32, no. 8, pp. 1598–1605.

**Peng, X. F.; Peterson, G. P.; Wang, B. X.** (1994): Frictional flow characteristics of water flowing through rectangular microchannels. *Experimental Heat Transfer*, vol. 7, no. 4, pp. 249–264.

**Qu, W.; Mudawar, I.** (2002): Experimental and numerical study of pressure drop and heat transfer in a single-phase microchannel heat sink. *Int.J. Heat Mass Transfer*, vol. 45, pp. 2549–2565.

**Rahman, M. M.** (2000): Measurements of heat transfer in microchannel heat sinks. *International Commun. Heat Mass Transfer*, vol. 27, no. 4, pp. 495–506.

**Reynaud, S.; Debray, F.; Franc, J. P.; Maitre, T.** (2005): Hydrodynamics and heat transfer in two-dimensional minichannels. *International Journal of Heat and Mass Transfer*, vol. 48, no. 15, pp. 3197–3211.

**Schlichting, H.; Gersten, K.** (2004): *Boundary layer theory*. Springer, 8th revised and enlarged revision edition.

**Yang, C. Y.; Wu, J. C.; Chien, H. T.; Lu, S. R.** (2003): Friction characteristics of water, r-134a, and air in small tubes. *Microscale Thermophys. Eng.*, vol. 7, no. 4, pp. 335–348.

**Yu, J.; Li, Z.; C. F. Ma, C. F.** (2006): Experimental study of pressure loss due to abrupt expansion and contraction in mini-channels. In *Proceedings of the 13th International Heat Transfer Conference*, Sydney. Begell House.

## Appendix A: Nomenclature

$D$	Diameter of the channel, $mm$
$L$	Length of the channel, $mm$
$L_e$	Length of establishment, $mm$
$U$	Velocity, $m/s$
$C_F$	Average friction factor
$d$	Small tube diameter, $mm$
$K_c$	Pressure loss coefficient

$l$	Small tube length, $mm$
$Lx1$	Upstream separation length, $\mu m$
$Lr1$	Upstream separation height, $\mu m$
$Lx2$	Downstream separation length, $\mu m$
$Lr2$	Downstream separation height, $\mu m$
$A$	Flow area, $mm^2$

Greek Symbols

$\mu$	Dynamic viscosity, Pa.s
$\rho$	Mass density, $kg/m^3$
$\nu$	Kinematic viscosity, $m^2/s$
$\delta$	Thickness of the dynamic boundary layer, $mm$
$\delta_{\tau\eta}$	Thickness of the thermal boundary layer, $mm$

Non-dimensional Numbers

$Re$	Reynolds number
$Nu$	Nusselt number
$P_o$	Poiseuille number, $[C_F, Re]$
$Pr$	Prandtl number
$y^+$	Non dimensional wall distance

